Vol. 4 • No. 13 • September 16 • 2015

www.advhealthmat.de

ADVANCED HEALTHCARE MATERIALS

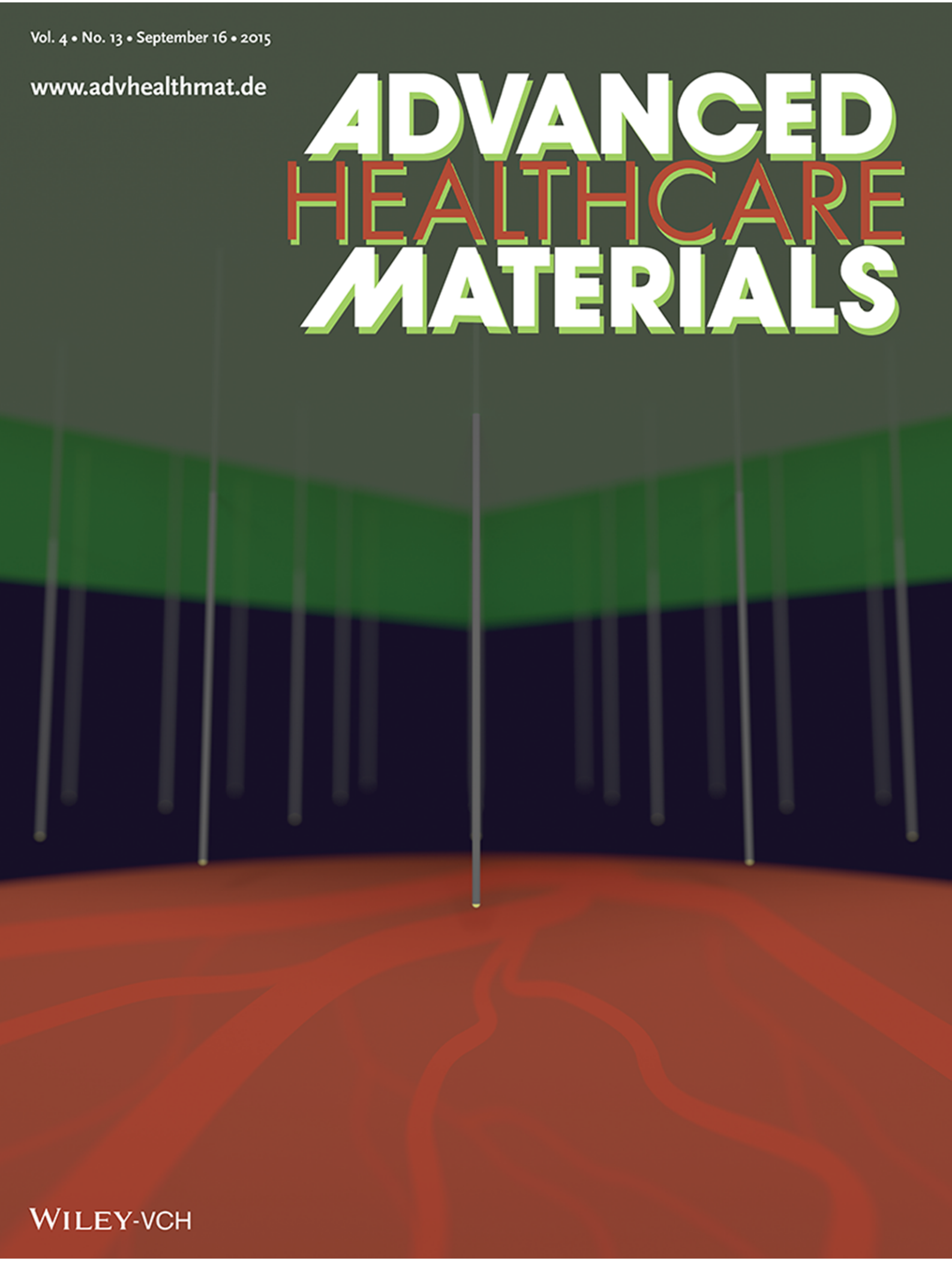

WILEY-VCH

ADVANCED HEALTHCARE MATERIALS
www.advhealthmat.de

Dissolvable Base Scaffolds Allow Tissue Penetration of High-Aspect-Ratio Flexible Microneedles

*Satoshi Yagi, Shota Yamagiwa, Yoshihiro Kubota, Hirohito Sawahata, Rika Numano, Tatsuya Imashioya, Hideo Oi, Makoto Ishida, and Takeshi Kawano**

Microscale-diameter, high-density needle array devices fabricated by microelectromechanical systems (MEMS) technology offer high spatiotemporal resolution electrophysiological recordings and stimulations,[1,2] drug delivery,[3] and optogenetics[4] on a large number of neurons in a tissue. Thus, MEMS-based microneedles have been used in numerous studies, including rodent-, monkey-, as well as human brains,[5,6] providing a fundamental understanding of these neuronal systems. Although such MEMS devices are powerful tools in neuroscience, the needle penetration-induced tissue/neuron damage remains problematic,[7–9] particularly in chronic and future medical applications.[5,6] One way to reduce the penetration damage is miniaturization of the needle diameter (or cross sectional area); low-invasive tissue penetrations have been demonstrated using needles <10 µm diameter (e.g., ≈8.5 µm diameter needle).[10] In addition, to address the mechanical mismatch between the penetrating needle and the brain/tissue, a needle with a flexible property is essential.[11,12] Future needle-device technology must combine these two features to expand neuroscience applications.

Vapor-liquid-solid (VLS)-grown silicon-needle array[13–16] is a way to address the aforementioned technological issues of microneedles. Compared to conventional MEMS-based needles, VLS silicon needles realize nano- to microscale needle diameters and a flexible property in silicon with a microscale diameter (Young's modulus of 188 GPa for <111> silicon). Although low-invasive tissue penetrations and in vivo neuronal action potential recordings have been confirmed using <7 µm diameter, 210 µm long VLS-needle arrays,[17,18] the tissue penetration capability of longer microneedles (>210 µm) must be investigated. However, increasing the needle length decreases the needle stiffness, which may cause the needle to buckle or fracture prior to penetration (**Figure 1**a). For example, 400 µm long silicon needles buckle in gelatin penetration tests.[19] To approach deep cell layers in a cortex, microneedles should be longer than 400 µm (e.g., ≈400 µm for the cortical layer IV in mouse brain and the cortical layer II in human brain).

To realize tissue penetration using high-aspect-ratio flexible microneedles, we propose an approach that "temporarily" enhances needle stiffness by embedding its base with a stiff film (hereafter referred to as a base scaffold), which dissolves upon contact with a biological tissue (e.g., brain). Although biocompatible silk[20,21] and polyethylene glycol (PEG)[12] are candidates for dissolvable materials, this study uses silk, which is prepared by simply dropping a silk solution over the needle's substrate and allowing it to dry for about a day. Compared to coating the entire needle with a dissolvable material,[20] the advantage of our approach is that the base scaffold does not increase the diameter (or cross sectional area) of the needle (e.g., <5 µm in diameter) in a tissue, reducing needle-induced tissue/neuron damage. Another advantage of the base scaffold without coating the needle is that the amount of the scaffold material diffused within the tissue is reduced. The silk scaffold dissolves and the amount of the silk solution diffuses over the surface of the tissue, but the silk solution is diluted and washed away by a solution (e.g., saline). Herein, we evaluate the effect of a silk-base scaffold on needle stiffness and the penetration capabilities using mouse brain. Both bending and tissue penetration tests indicate that the proposed base scaffold improves the penetration capability of high-aspect-ratio flexible microneedles.

We demonstrate tissue penetrations of microneedles using a base scaffold of silk fibroin. Silk fibroin is a candidate dissolvable material because it is biocompatible, water soluble with programmable rates, and easy-to-use, especially for coatings of vertically assembled microneedle arrays. The dissolution speed of the silk fibroin in contact with water is on the order of the 50% in volume per 10 min.[21]

Increasing the aspect ratio of a needle reduces the longitudinal stiffness of the needle itself, resulting in buckling or fracturing of the needle prior to penetration (Figure 1b). The buckling load of a needle with a column shape can be expressed as

$$F_{\text{Buckle}} = \frac{2\pi EI}{l^2} \propto E\left(\frac{1}{l}\right)^2 \quad (1)$$

$$I = \frac{\pi d^2}{64} \quad (2)$$

where F_{Buckle} is the buckling load, E is Young's modulus, l is the needle length, I is the cross-sectional second-order moment,

S. Yagi, S. Yamagiwa, Y. Kubota, Prof. H. Sawahata, T. Imashioya, Prof. M. Ishida, Prof. T. Kawano
Department of Electrical and Electronic Information Engineering
Toyohashi University of Technology
1-1 Hibarigaoka, Tempaku-cho
Toyohashi 441-8580, Japan
E-mail: kawano@ee.tut.ac.jp
Prof. R. Numano
Department of Environmental and Life Sciences
Toyohashi University of Technology
1-1 Hibarigaoka, Tempaku-cho, Toyohashi 441-8580, Japan
Prof. R. Numano, Prof. H. Oi, Prof. M. Ishida
Electronics-Inspired Interdisciplinary Research Institute (EIIRIS)
Toyohashi University of Technology
1-1 Hibarigaoka, Tempaku-cho, Toyohashi 441-8580, Japan

DOI: 10.1002/adhm.201500305

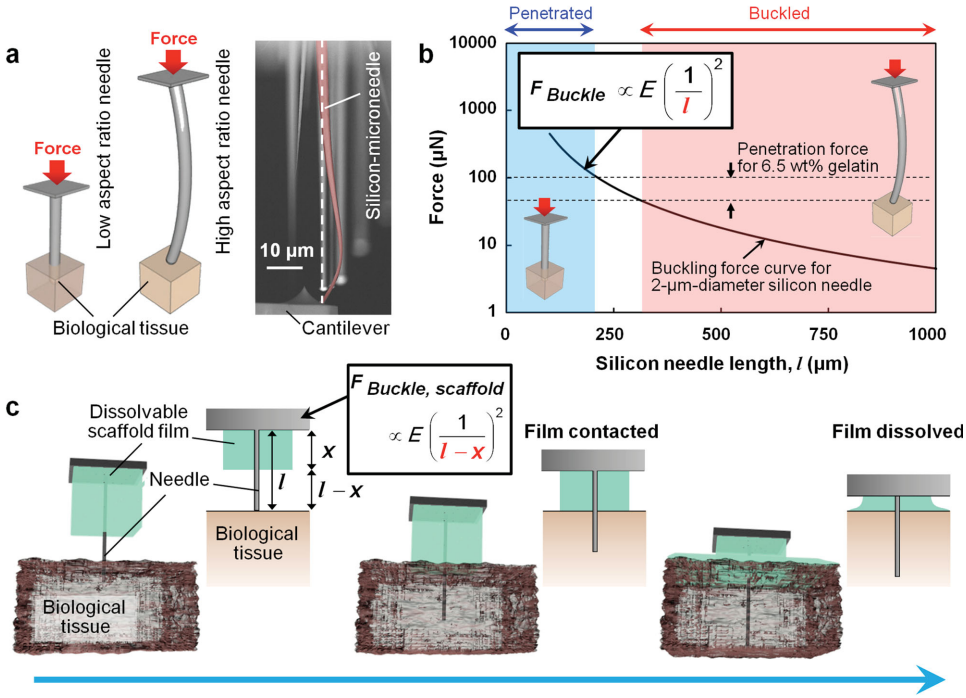

Figure 1. Concept for tissue penetration of a high-aspect-ratio, flexible needle using a dissolvable base scaffold. a) Schematics showing that increasing the needle length reduces the needle stiffness, resulting in buckling prior to tissue penetration. SEM image showing a buckled silicon microneedle with a compressing force. b) Buckling-load–needle-length curve for a silicon microneedle. Curve is from buckling tests on 2 μm diameter VLS-grown silicon needles and a theoretical model. Graph, which also includes the experimentally measured penetration force for gelatin (6.5 wt% in water), shows two regimes: a needle with a buckling force that exceeds the penetration force results in penetration (blue) and a needle with a buckling force lower than that of the penetration force results in buckling prior to penetration (red). c) Procedure for tissue penetration of a high-aspect-ratio flexible microneedle using a dissolvable base scaffold. Embedding the needle base with a stiff base scaffold film (thickness, *x*) "temporarily" increases the buckling force of the needle (length, *l*), but the film dissolves upon contact with a biological tissue (e.g., brain).

and d is the needle diameter. The buckling load is proportional to $1/l^2$, indicating that increasing the needle length decreases the buckling force itself. When the buckling force is less than the required penetration force, the needle buckles before the tissue is punched. Thus, the stiffness of high-aspect-ratio microneedles is essential to achieve the tissue penetration.

A silk film, which covers the base of the needle, acts as a mechanical support for the needle base and decreases the length of the flexible portion of the microneedle (Figure 1c), and the buckling force can be expressed as

$$F_{\text{Buckle,scaffold}} \propto E\left(\frac{1}{l-x}\right)^2 \quad (3)$$

where x is the thickness of the silk film. Equation (1) indicates that the buckling load of the silk-embedded needle is proportional to $1/(l-x)^2$, which increases the buckling force compared to that without the silk scaffold [Equation (1)].

High-aspect-ratio flexible silicon microneedles buckle before needle penetration.[19] Vertical <111> silicon microneedles (Young's modulus of 188 GPa) were prepared on a (111) silicon substrate by gold (Au)-catalyzed VLS growth of silicon.[22] Figure 1b includes the buckling-load–needle-length curve obtained via experimental buckling tests on 2 μm diameter VLS-grown silicon needles using a tungsten needle (diameter >> 2 μm) and a theoretical model (Figure S1, Supporting Information). In addition, the experimentally measured penetration force (45–100 μN) for a mechanical tissue phantom of gelatin (6.5 wt% in water) is shown, suggesting that 2 μm diameter silicon needles longer than ≈250 μm buckle prior to gelatin penetration. Because the actual brain stiffness depends on the sample (e.g., age dependence for rat brain),[23] we used a tissue phantom of gelatin (6.5 wt% in water), which is slightly stiffer than brain tissue.

To form the silk-film scaffold at the needles' base, a silk solution (silk protein extract, Matsuda Farm) was dropped over the silicon-needle substrate followed by crystallization of the silk solution in air within one day (**Figure 2**a,b). Due to the growth yield of the vertically aligned high-aspect-ratio needles, the array (lower picture in Figure 2a) consists of a site without needles and needles with different growth directions. By eliminating the irregular needles, all the results in this work are discussed using vertically aligned high-aspect-ratio needles. The actual silicon needle used in tissue penetration was encapsulated with a biocompatible material of parylene (1 μm thick) prior to silk formation. Because the surface tension and contraction stress of the silk solution cause the needles to bend, the silk was crystallized/dried with the surface of the needle substrate facing down. This crystallization/drying process reduces the forces/stresses due to the force of gravity, causing the needle not to bend (Figure S2, Supporting Information).

Adv. Healthcare Mater. **2015**,
DOI: 10.1002/adhm.201500305

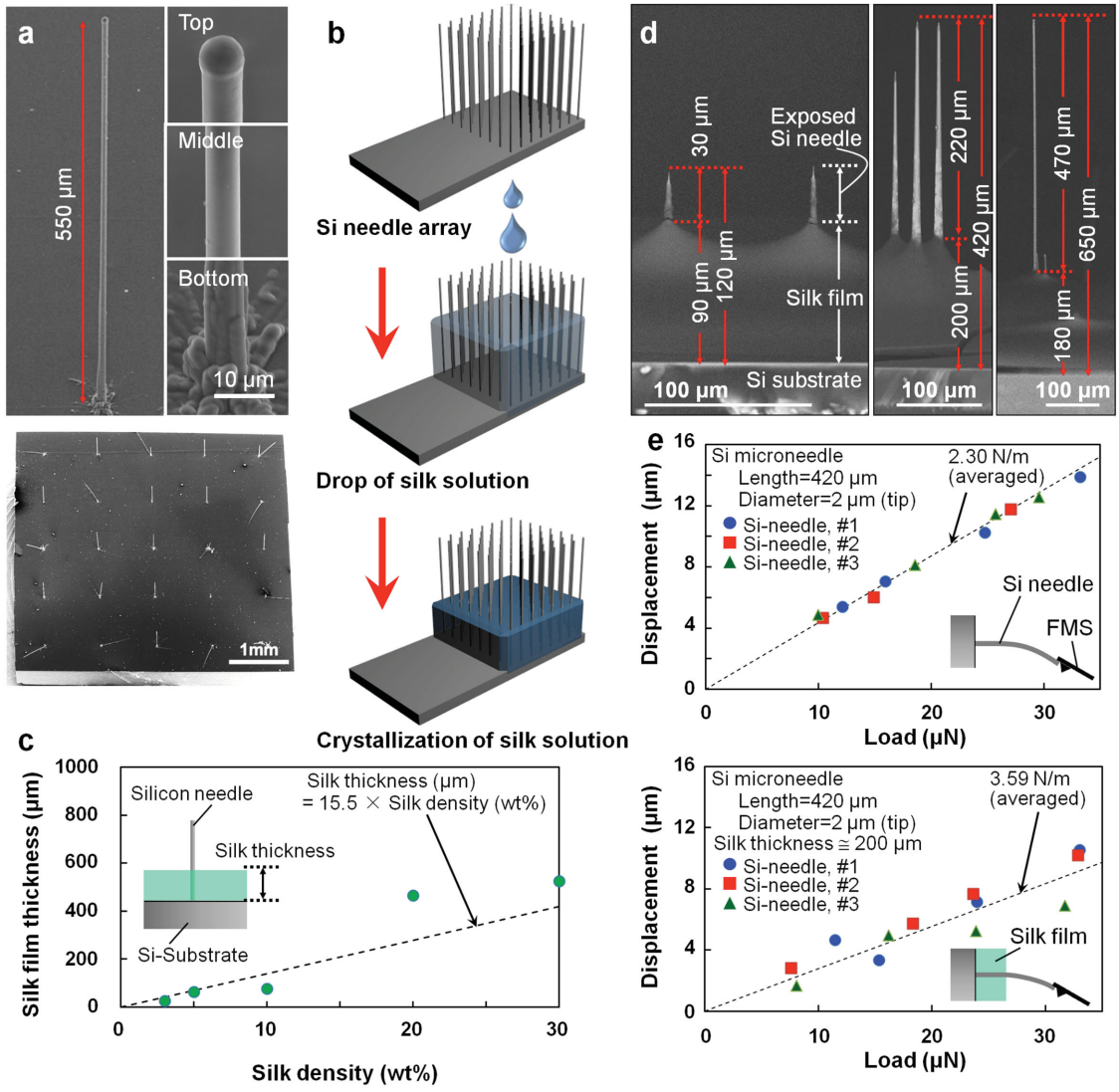

Figure 2. Silk film-base scaffold for high-aspect-ratio flexible VLS-grown silicon microneedles. a) SEM images of an individual silicon microneedle with a 550 µm length and ≈5 µm diameter (upper panels) and a device chip consisting of an array with 5 × 5 needle sites (bottom). b) Schematics of the steps for the silk-base scaffold film. Silk solution is dropped over the silicon-needle substrate followed by crystallization of the silk solution in air within 1 d. c) Silk film thickness is controlled by the silk density. Plots are taken from the 5 mm × 5 mm dipping area a) with a constant amount of the silk solution of 37.5 mm^3. Dashed line represents the average value from five measurement points. d) SEM images showing the silk-embedded silicon microneedles: 120 µm long needles with the 90 µm thick silk film (left), 420 µm long needles with the 200 µm thick silk film (center), and a 650 µm long needle with the 180 µm thick silk film (right). e) Bending tests of silicon microneedles. Displacement–load characteristics for 420 µm long, 2 µm tip-diameter silicon needles without the silk-film scaffold (top) and with the ≈200 µm thick silk-film scaffold (bottom).

The thickness of the crystallized silk film depends on the silk density in solution. Herein, the silk solution of 37.5 mm^3 for 5 mm × 5 mm dipping area was used to investigate the silk-thickness–silk-density curve (Figure 2c). The thicknesses of the silk scaffold, which ranged from ≈90 to ≈200 µm, were prepared for 120, 420, and 650 µm long needles, while the needles' bases were embedded in the silk scaffold (Figure 2d). The silk at the needle base is tapered due to the surface tension between the silk and the needle (parylene for the outer shell of the silicon needle). To completely coat the needle with silk, increasing the silk density can increase the thickness of the silk scaffold (Figure 2c); we have confirmed that the entire ≈200 µm long needle can be coated without bending the needle.

The needle bending tests confirmed the increased stiffness of the silk-embedded silicon microneedles. The displacement–load characteristics of the needle were measured by a force measurement system (FMT-120, Kleindiek Nanotechnik, Reutlingen, Germany) inside a scanning electron microscope (SEM) chamber. Figure 2e shows the displacement–load curves taken from 420 µm long, 2 µm tip-diameter silicon needles without and with the silk-film scaffold, respectively. The thickness of silk at the needle's base is ≈200 µm, indicating that a ≈220 µm long needle section is exposed from the silk. The stiffness of the silicon needle without a silk-film scaffold is 2.30 N m^{-1}, but increases to 3.59 N m^{-1} for a silk-embedded silicon needle. The improved stiffness is given by 3.59 (N m^{-1})/2.30 (N m^{-1}) ≅ 156%,

which is similar to the simulated value (Figure S3, Supporting Information). The stiffness of the silk-embedded needle is consistent with that of a 220 μm long silicon needle with the same diameter (2 μm tip diameter), indicating that bending is mainly due to the needle section exposed from the silk-film scaffold.

The penetration capability of the silk-embedded silicon microneedle was confirmed using mouse brain. For the animal experiments, we used a 5 × 5 needle array (needle interval = 1 mm) on a 5 mm × 5 mm silicon substrate (Figure 2a), which die size allows the needle array to manipulate and penetrate the brain of a mouse. Herein, the length and diameter of the silicon needle were 650 and 5 μm, respectively, and the thickness of the silk film at the needle base was 260 μm (390 μm long needle section exposed from the silk). The penetration of the silk-embedded microneedle was conducted using the whole brain extracted from a mouse (27 g weight), which was euthanized by cervical dislocation. After removing the dura, the microneedle array penetrated into the somatosensory area (barrel area, 2–4 mm lateral and 0–2 mm caudal from bregma) in the right hemisphere of the brain. The position of the needle array was controlled by an *x*–*y*–*z* remote manipulator system, while the instantaneous penetration was observed using a microscope (VH-Z100, Keyence, Osaka, Japan). During the manipulation of the needle toward the brain, the needle without the silk-scaffold buckles (≈6 s in **Figure 3**a, and Movie S1 in the Supporting Information), and the needle did not penetrate into the brain (6–12 s in Figure 3a). On the other hand, the needle with the silk-scaffold punched the surface of the brain (10–20 s in Figure 3b, and Movie S2, Supporting Information), the silk-base scaffold made contact with the brain surface (≈50 s in Figure 3b), and the needle penetrated into the brain without the needle buckling. After coming into contact with the brain surface (≈50 s in Figure 3b), the silk dissolved, exposing the entire needle section. In this scheme, >80 vol% silk film dissolved after >15 min.

To expand the in vivo applications, the penetration capability of the silk-embedded needle was also confirmed using the mouse brain in vivo (**Figure 4**). The stiffness/pressure of the mouse brain in the skull is higher than that of the aforementioned extracted whole brain (Figure 3). The significant difference in the needle penetration between the whole brain and the brain in vivo is the pulsatile motion of the brain. The in vivo brain penetrations of the microneedles were demonstrated using a mouse (25 g weight), which was deeply anesthetized with urethane (50 μL of 30% solution/10 g body weight). In addition to needle penetration, the drug/chemical delivery capability of the needle was confirmed by injecting nanoparticles during needle penetration. Due to the surface energy between the particle (polystyrene) and the needle (parylene), particles spread over the brain surface can be trapped with the needles and then delivered into the brain upon needle penetration.[24] After removing the dura, polystyrene particles [Merck

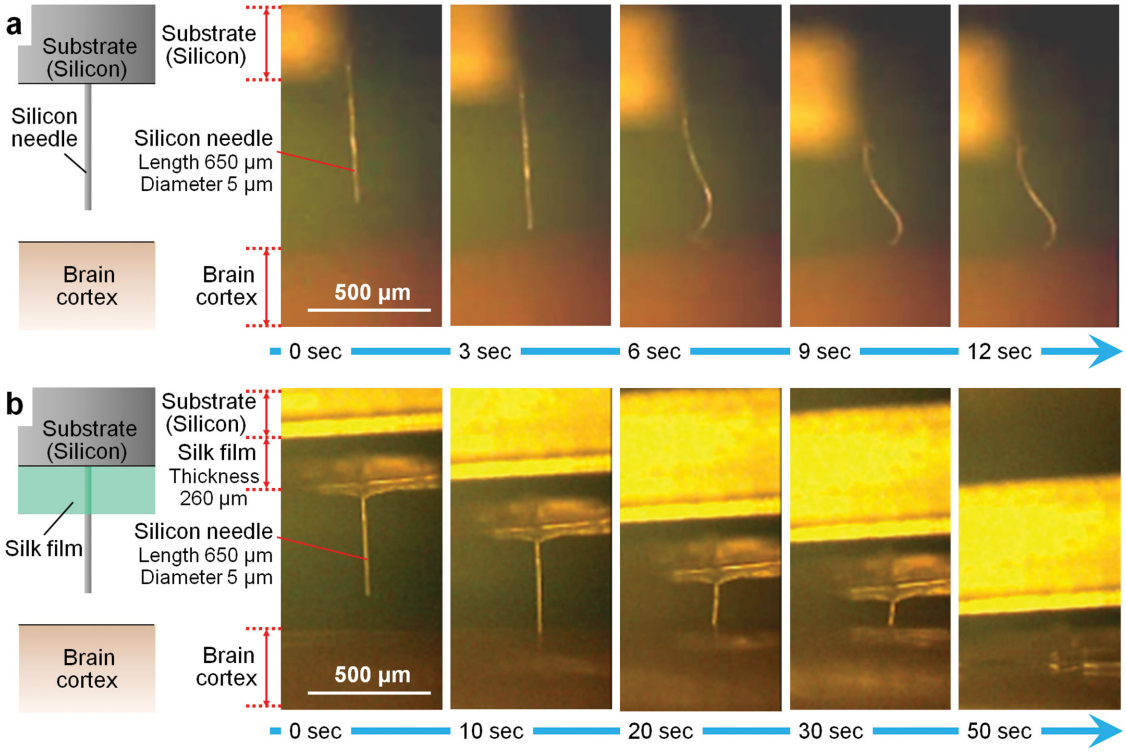

Figure 3. Penetration capability of the silicon microneedle with and without the silk-base scaffold film using the whole brain extracted from a mouse. a) Schematic and picture panels showing a silicon microneedle without the silk film for brain penetration. Needle buckles prior to penetration of the mouse brain (≈6 s) (Movie S1, Supporting Information). b) Schematic and picture panels showing a silk-embedded silicon microneedle during needle penetration into mouse brain (Movie S2, Supporting Information). Needle penetrates the brain without buckling. Silk film dissolves after contact with the brain (≈50 s). Length and diameter of the used silicon needles in (a) and (b) are 650 and 5 μm, respectively. Silk-film thickness at the needle base is 260 μm b). Position of the silicon needles within a 5 mm × 5 mm substrate is controlled by an *x*–*y*–*z* remote manipulator system.

Adv. Healthcare Mater. **2015**,
DOI: 10.1002/adhm.201500305

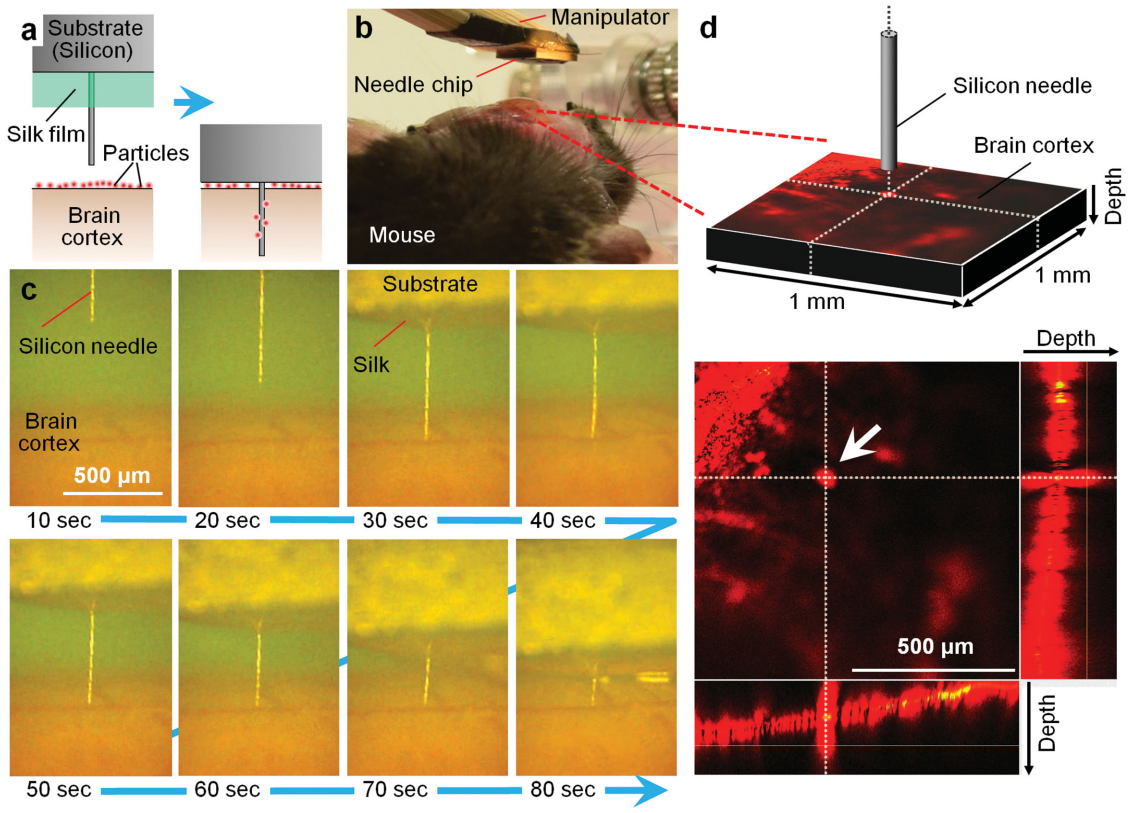

Figure 4. Penetration of silk-embedded silicon microneedles and injections of particles into in vivo mouse brain. a) Schematics for particle injections via the silicon microneedle. b) Photograph of the set up for the in vivo mouse brain experiments. 5 mm × 5 mm silicon-needle-array substrate is positioned over the brain by an *x*–*y*–*z* remote manipulator system. c) Panels depicting a silicon needle during needle penetration and particle injection (Movie S3, Supporting Information). Pictures include needle contact with the brain (≈30 s), needle penetration (30–60 s), and silk contact and the dissolution (≈80 s). Length and diameter of the silicon needle are 650 and 5 µm, respectively, and the thickness of the silk film at the needle base is 260 µm. d) Schematic and confocal microscope images of the particles injected into the brain. Particle emissions are observed in the brain between a ≈270 µm depth and the surface.

F1-XC050, modified with COOH, excitation wavelength = 470, 480, and 490 nm, emission wavelength = 525 and 560 nm, particle diameter = 506 nm ± (standard deviation = 6 nm)] for the injection were spread over the brain surface.

Similar to the aforementioned whole brain penetration, the microneedle array penetrated into the somatosensory area (barrel area, 2–4 mm lateral and 0–2 mm caudal from bregma) in the right hemisphere of the brain in vivo. Although the pulsatile motion of the brain occurs during penetration, the silk-embedded needles allow the brain to be penetrated without fracturing the needle (Figure 4c, and Movie S3, Supporting Information). Particle injections (or needle penetrations) were conducted more than six times on the somatosensory area of the brain. The particle injection (or needle penetration) sites in the brain were determined by confirming particle emission in confocal microscope observations (Laser Confocal Microscopy A1, Nikon, Laser excitation wavelength = 488 nm, emission filter = 595/50 nm for signal detection from deep particles). The confocal microscope observations confirm that the particle emission sites are consistent with the areas where microneedles penetrate. The particle emissions are observed in the brain between the surface and a depth of ≈270 µm (Figure 4d). Although the microneedles allow particles to be injected into the brain, the depths of the injected particles are shallower than the length of the microneedles (650 µm long). The results suggest that the particles are released from the microneedles before the needles are fully inserted due to the higher surface energy at the particle/tissue (brain) interface than that of the particle/microneedle.[24] Because light scattering of both excitations and emissions in brain tissue limits the imaging depth in confocal microscopy, further analysis is necessary to discuss the depth of the injected nanoparticles (e.g., preparation of brain slices, two-photon microscope observations of injected nanoparticles, and preparation of transparent brain tissue[25,26]).

The controllability of the dissolution speed is an important characteristic of the silk scaffold in the proposed scheme. As demonstrated in the needle penetration into mouse brain, >80 vol% silk film dissolves after 15 min, which is sufficient to expose the needle from the brain-contacted silk (260 µm thick) and allow the needle to penetrate the brain. However, the time required to dissolve the silk scaffold depends on the application. Although we demonstrated the same silk composition for a dissolution speed (80 vol% dissolved for 15 min), the dissolution time can be increased to days or weeks using water or methanol-treated silk films.[21,27] As previously mentioned, PEG is another candidate for the base scaffold material, which is also dissolvable and biocompatible. Additionally, changing the molecular weight of PEG should alter the dissolution speed of PEG.

The silk-embedded silicon microneedles penetrate mouse brain, confirming that the silk scaffold increases the needle's stiffness, enabling needle penetration. To prevent the needle tip from slipping on the tissue surface, it is important that the needle penetration is perpendicular to the surface of the target tissue. A needle slip induces movement of the needle tip from the initial point, decreasing the buckling force of the needle, which is given as

$$F_{\text{Buckle,scaffold}} \propto E\left[\frac{1}{K(l-x)}\right]^2 \quad (4)$$

where K is the column effective length factor. If slipping the needle tip over the brain is negligible, then the buckling force of the needle can be discussed with a model where one end is fixed (needle end with silk) and the other end is pinned (and in contact with the brain surface), representing $K \cong 0.699$ in Equation (4). We confirmed the pinned needle tip in the buckling observation with a cantilever and the needle penetration into whole mouse brain (SEM image in Figure 1a and pictures in Figure 3a).

Once the needle tip slips/moves over the brain, the buckling load decreases with $K = 2$, which is represented by a model where one end is fixed (needle end with silk) and the other end moves freely (the free end slips/moves over the brain). In actual needle penetrations, brain and other biological tissues have hemispherical shapes, making perpendicular needle penetration difficult, especially when using a needle array with an interval (e.g., 1 mm needle interval for an 5 × 5 mm die size as shown in Figure 2a) and/or the brain/tissue with a curvature radius such as a mouse brain as demonstrated in our penetrations (Figures 3 and 4). Although both mouse brains have a small curvature hemispherical shape and the microneedles are not manipulated perpendicularly to the brain surfaces, the proposed silk-base scaffold realizes microneedles with a sufficient stiffness for penetration. In the future, a nanoscale needle tip may improve the effectiveness of needle penetration.[24,28] A nanoscale tipped microneedle can punch and be fixed onto the brain surface before the needle penetrates without decreasing the buckling force of the needle itself [$K \cong 0.5$ in Equation (4)].

As a step toward future applications, including electrophysiological recordings and stimulations, drug delivery, and optogenetics, here we demonstrate >500 μm long silk-embedded flexible needle penetrations using mouse brain. Compared to conventional needles with larger diameters, our <5 μm diameter needles have the potential to reduce the invasiveness and provide safer tissue penetration. However, microneedles must possess numerous functionalities for diverse applications. Microfabrication processes are promising in this regard. Electrical recording microneedles can be fabricated by 3D needle metallization and insulation.[17,18] For neural stimulation applications, we have developed a low-impedance and high-charge-injecting electrode material composed of layer-by-layer assembled iridium oxide/platinum black, which can be deposited at the electrode site.[29] In addition, the particle delivery into mouse brain as demonstrated here is applicable to numerous drug/chemical delivery applications by simply modifying these particles with chemicals/molecules. We have developed tube-like microscale needles for drug delivery[30] and optogenetic applications.[31,32] The proposed silk scaffold can be used to improve the penetration capability of these microtubes with a high-aspect-ratio and flexible property.

We propose employing a dissolvable silk-base scaffold to enhance the stiffness of the high-aspect-ratio flexible microneedles, discuss the effect of the scaffold on the increased stiffness of the silicon microneedles by bending tests, and demonstrate the penetration capabilities using whole mouse brain and the mouse brain in vivo. Compared to the other methodologies, such as coating the entire needle with a dissolvable material, the proposed base scaffold does not increase the needle diameter, providing low invasive tissue penetrations of flexible microscale-diameter needles. Although the effect of silk-base scaffold is demonstrated using silicon microneedles, this approach is applicable to numerous other high-aspect-ratio flexible needles, including in vivo/in vitro electrophysiological stimulation- and recording-electrodes, drug/chemical delivery pipettes, and optogenetic fibers. This approach should reduce the invasiveness and provide safer tissue penetration compared to conventional approaches.

Experimental Section

Animal Experiments: All experimental procedures using mice and animal care were approved by the animal experiments committee of Toyohashi University of Technology.

Supporting Information

Supporting Information is available from the Wiley Online Library or from the author.

Acknowledgements

This work was supported by Grants-in-Aid for Scientific Research (S) (No. 20226010), (A) (No. 25249047), for Young Scientists (A) (No. 26709024), and the PRESTO Program from JST. R.N. was also supported by a Grant-in-Aid for Scientific Research (C) (No. 24590350) and the Takeda Science Foundation.

Received: April 24, 2015
Revised: June 13, 2015
Published online:

[1] K. Najafi, K. D. Wise, T. Mochizuki, *IEEE Trans. Electron Devices* **1985**, *ED-3*, 1206.
[2] P. K. Campbell, K. E. Jones, R. J. Huber, K. W. Horch, R. A. Normann, *IEEE Trans. Biomed. Eng.* **1991**, *38*, 758.
[3] L. Lin, A. P. Pisano, *J. Microelectromech. Syst.* **1999**, *8*, 78.
[4] J. Zhang, F. Laiwalla, J. A Kim, H. Urabe, R. V. Wagenen, Y. Song, B. W. Connors, F. Zhang, K. Deisseroth, A. V. Nurmikko, *J. Neural Eng.* **2009**, *6*, 055007.
[5] L. R. Hochberg, M. D. Serruya, G. M. Friehs, J. A. Mukand, M. Saleh, A. H. Caplan, A. Branner, D. Chen, R. D. Penn, J. P. Donoghue, *Nature* **2006**, *442*, 164.
[6] L. R Hochberg, D. Bacher, B. Jarosiewicz, N. Y Masse, J. D. Simeral, J. Vogel, S. Haddadin, J. Liu, S. S. Cash, P. van der Smagt, J. P. Donoghue, *Nature* **2012**, *485*, 372.

[7] D. H. Szarowski, M. D. Andersen, S. Retterer, A. J. Spence, M. Isaacson, H. G. Craighead, J. N. Turner, W. Shain, *Brain Res.* **2003**, *983*, 23.
[8] R. Biran, D. C. Martin, P. A. Tresco, *Exp. Neurol.* **2005**, *195*, 115.
[9] V. S. Polikov, P. A. Tresco, W. M. Reichert, *J. Neurosci. Methods* **2005**, *148*, 1.
[10] T. D. Kozai, N. B. Langhals, P. R. Patel, X. Deng, H. Zhang, K. L. Smith, J. Lahann, N. A. Kotov, D. R. Kipke, *Nat. Mater.* **2012**, *11*, 1065.
[11] S. Takeuchi, T. Suzuki, K. Mabuchi, H. Fujita, *J. Micromech. Microeng.* **2004**, *14*, 104.
[12] S. Takeuchi, D. Ziegler, Y. Yoshida, K. Mabuchi, T. Suzuki, *Lab Chip* **2005**, *5*, 519.
[13] T. Kawano, Y. Kato, M. Futagawa, H. Takao, K. Sawada, M. Ishida, *Sens. Actuator A* **2002**, *97*, 709.
[14] T. Kawano, Y. Kato, R. Tani, H. Takao, K. Sawada, M. Ishida, *IEEE Trans. Electron Devices* **2004**, *51*, 415.
[15] T. Kawano, T. Harimoto, A. Ishihara, K. Takei, T. Kawashima, S. Usui, M. Ishida, *Biosens. Bioelectron.* **2010**, *7*, 1809.
[16] A. Okugawa, K. Mayumi, A. Ikedo, M. Ishida, T. Kawano, *IEEE Electron Device Lett.* **2011**, *32*, 683.
[17] A. Fujishiro, H. Kaneko, T. Kawashima, M. Ishida, T. Kawano, presented at *IEEE 24th Int. Conf. on Micro Electro Mechanical Systems (MEMS)*, Cancun, Mexico, France, January **2011**.
[18] A. Fujishiro, H. Kaneko, T. Kawashima, M. Ishida, T. Kawano, *Sci. Rep.* **2014**, *4*, 4868.
[19] S. Morita, A. Fujishiro, A. Ikedo, M. Ishida, T. Kawano, presented at *IEEE 25th Int. Conf. on Micro Electro Mechanical Systems (MEMS)*, Paris, France, January **2012**.
[20] L. W. Tien, F. Wu, M. D. Tang-Schomer, E. Yoon, F. G. Omenetto, D. L. Kaplan, *Adv. Funct. Mater.* **2013**, *23*, 3185.
[21] D. H. Kim, J. Viventi, J. Amsden, J. Xiao, L. Vigeland, Y.-S. Kim, J. A. Blanco, B. Panilaitis, E. S. Frechette, D. Contreras, D. L. Kaplan, F. G. Omenetto, Y. Huang, K.-C. Hwang, M. R. Zakin, B. Litt, J. A. Rogers, *Nat. Mater.* **2010**, *9*, 511.
[22] A. Ikedo, T. Kawashima, T. Kawano, M. Ishida, *Appl. Phys. Lett.* **2009**, *95*, 033502.
[23] A. Gefen, N. Gefen, Q. Zhu, R. Raghupathi, S. S. Margulies, *J. Neurotrauma* **2003**, *20*, 1163.
[24] A. Goryu, R. Numano, A. Ikedo, M. Ishida, T. Kawano, *Nanotechnology* **2012**, *23*, 415301.
[25] K. Chung, J. Wallace, S. Y. Kim, S. Kalyanasundaram, A. S. Andalman, T. J. Davidson, J. J. Mirzabekov, K. A. Zalocusky, J. Mattis, A. K. Denisin, S. Pak, H. Bernstein, C. Ramakrishnan, L. Grosenick, V. Gradinaru, K. Deisseroth, *Nature* **2013**, *497*, 332.
[26] M. T. Ke, S. Fujimoto, T. Imai, *Nat. Neurosci.* **2013**, *16*, 1154.
[27] H.-J. Jin, J. Park, V. Karageorgiou, U.-J. Kim, R. Valluzzi, P. Cebe, D. L. Kaplan, *Adv. Funct. Mater.* **2005**, *15*, 1241.
[28] A. Goryu, R. Numano, A. Ikedo, M. Ishida, T. Kawano, *Nanotechnology* **2010**, *21*, 125302.
[29] S. Yamagiwa, A. Fujishiro, H. Sawahata, R. Numano, M. Ishida, T. Kawano, *Sens. Actuator B* **2015**, *206*, 205.
[30] K. Takei, T. Kawashima, T. Kawano, H. Kaneko, K. Sawada, M. Ishida, *Biomed. Microdevices* **2009**, *11*, 539.
[31] M. Sakata, T. Nakamura, T. Matsuo, A. Goryu, M. Ishida, T. Kawano, *Appl. Phys. Lett.* **2014**, *104*, 164101.
[32] K. Takei, T. Kawano, T. Kawashima, K. Sawada, H. Kaneko, M. Ishida, *Biomed. Microdevices* **2010**, *25*, 1809.